Vortex formation in neutron-irradiated rotating superfluid ^{3}He-B

A.P. Finne[*], **S. Boldarev**[*,†], **V.B. Eltsov**[*,†], **and M. Krusius**[*]

[*]*Low Temperature Laboratory, Helsinki University of Technology,*
P.O. Box 2200, FIN-02015 HUT, Finland
[†]*Kapitza Institute for Physical Problems, 119334 Moscow, Russia*

A convenient method to create vortices in meta-stable vortex-free superflow of ^{3}He-B is to irradiate with thermal neutrons. The vortices are then formed in a rapid non-equilibrium process with very distinctive characteristics. Two models were suggested to explain the phenomenon. One is based on the Kibble-Zurek mechanism of defect formation in a quench-cooled second order phase transition. The second model builds on the instability of the moving front between superfluid and normal ^{3}He, which is created by the heating from the neutron absorption event. The most detailed measurements with single-vortex resolution have been performed at temperatures close to T_c. We present an overview of the main experimental features and demonstrate that the measurements are consistent with the Kibble-Zurek picture. New data, collected at low temperatures, support this conclusion, but display superfluid turbulence as a new phenomenon. Below $0.6\,T_c$ the damping of vortex motion from the normal component is reduced sufficiently so that turbulent vortex dynamics become possible. Here a single absorbed neutron may transfer the sample from the meta-stable vortex-free to the equilibrium vortex state. We find that the probability for a neutron to initiate such a turbulent transition grows with increasing superflow velocity and decreasing temperature.

PACS numbers: 47.32, 67.40, 67.57, 98.80

1. NON-EQUILIBRIUM PHASE TRANSITIONS

Exposure to radiation causes changes in the structure of matter – radiation damage – which depends on the type of radiation and the absorbing material. Defects are produced, which may range from nuclear reactions to ionization and other non-elastic scattering effects. The interaction products

then have to be accommodated in the structure of the material which leads to a multitude of different phenomena. In superconductors and superfluids absorption events from applied radiation induce defects also in the spatial distribution of the order parameter. If the state of such a coherent many-body system is close to a critical point, for instance in a superfluid in the regime where the flow may intermittently switch between laminar and turbulent, the life time of the laminar state has been found to be limited by the background radiation level of the laboratory surroundings.[1] We discuss here a similar case where applied ionizing radiation is found to create quantized vortex lines in meta-stable superflow which is originally prepared to be vortex-free.[2] Depending on conditions, one irradiation event may produce from zero to a few vortex lines, or it may suddenly send the sample to the equilibrium vortex state, producing thousands of vortices.

An ionization event leads to heating where some small volume of the superfluid is abruptly heated above T_c to the normal state. The subsequent cool down of this warm bubble back to the superfluid state is an example of a rapid phase transition in conditions far from equilibrium. In 1976 Tom Kibble proposed that the inhomogeneous distribution of visible matter in the universe – known as the large-scale structure – might originate from defects which are formed in a rapid 2nd order phase transition during the early expansion and cooling after the Big Bang.[3] The defect formation transforms the original homogeneous system into an inhomogeneous. This suggestion was augmented by Wojciech Zurek in 1985 with quantitative predictions for the density of the defects, using scaling arguments about the slowing down of the order-parameter relaxation at the critical point.[4] Since then, cosmic strings have not been found and measurements on the angular distribution of the anisotropy in the cosmic background radiation have supported another explanation – the inflation model – as the origin of large-scale structure.

In condensed matter physics the Kibble-Zurek (KZ) mechanism of defect formation has remained an important issue: Are there real laboratory examples in which this mechanism can be proven to work? Phase transitions in condensed-matter systems are more often than not connected with defect formation. This is ascribed to different inhomogeneities of the system, such as impurities, grain boundaries, surfaces, etc. Superfluid ^{3}He-B was perhaps the first system where the KZ mechanism has been difficult to dispute,[2,5–7] the match between experiment and model looks perfect. However, solid theoretical justification is still missing which would prove the process in superfluid ^{3}He-B with a detailed microscopic calculation.

Ions in superfluid ^{4}He-II can be accelerated with electric fields to produce vortex rings.[8] The ions formed in applied radiation can thus be assumed to be directly responsible for the vortex production if electric fields

are present. This is assumed to be the case in Ref. 1. In zero applied electric field the experimental situation in ^{4}He-II is controversial,[9] while in ^{3}He-B irradiation with neutrons at thermal wave lengths has become a useful tool for creating vortex lines in vortex-free superflow.

In liquid ^{3}He the mean length of flight of a thermal neutron is ~ 0.1 mm, before the neutron undergoes the capture reaction n + $^3_2$He $\rightarrow$ p + $^3_1$H + 764 KeV. The reaction products, the proton and the triton, carry the kinetic energy of 764 keV and produce a cascade of ionizations among the surrounding ^{3}He atoms. The ionization processes and the resulting heating are restricted to a volume of less than 0.1 mm in diameter. The heated bubble cools back to the temperature of the surrounding superfluid bath within microseconds. Thus the heating occurs locally within the bulk superfluid, but close to the outer boundary of the cylindrical sample (with radius R). In rotation at the angular velocity Ω this is the place with a well-defined superflow velocity, $v_s = \Omega R$, the largest possible value. If this superflow velocity exceeds some critical value, then vortices are observed to emerge from a single neutron absorption event. In practice the process has turned out to be a conveniently controllable method to form vortices. Its critical velocity is unaffected by the surface properties of the sample container. If other critical velocities happen to be unattainably high, neutron radiation can always be used to create vortices in a predictable way. Experimentally a major advantage of neutrons over other types of radiation, such as γ rays, is that temperature stability can be maintained without any effort, since neutron absorption elsewhere in the apparatus is insignificant.

This report is divided in two main sections. The first contains an analytic model of the KZ mechanism which is then compared to experiment in the high temperature regime ($0.80\,T_c < T < T_c$) where the measurements have been most extensive.[2,10] The second section reports on new experiments below $0.60\,T_c$. Our measurements are performed with NMR techniques. In the high temperature range the vortex line count can be carried out with single-vortex resolution. The vortex dynamics in this temperature range is severely damped by mutual friction and is reasonably well understood. Thus it is possible to trace the connection between the initial configuration of vortices after the neutron absorption event and their final number as rectilinear lines in rotation. Here the agreement between the KZ model and the experiment is at least semi-quantitative. In contrast, below $0.60\,T_c$ the injection of the vorticity by the neutron absorption event sends the ^{3}He-B sample with some probability for a short transitory period into a turbulent state, where the number of vortices rapidly multiplies. After the relaxation of the turbulence, the final stable state is the equilibrium vortex state. In this process the initial configuration of vortices after the neutron absorption

event is sufficient to trigger the turbulence and is thus not directly related to the final number of rectilinear lines.

2. MODEL OF VORTEX FORMATION

2.1. Defect formation in a non-equilibrium phase transition

A homogeneous thermal quench through the transition temperature $T_{\rm c}$ is characterized in the KZ model[4] by one experimental variable, the quench time

$$\tau_{\rm Q} = \left(\frac{1}{T_{\rm c}} \left| \frac{dT}{dt} \right|_{T=T_c} \right)^{-1} , \tag{1}$$

so that the temperature evolution $T(t)$ at $T_{\rm c}$ can be approximated with a linear dependence $T = T_{\rm c}(1 - t/\tau_{\rm Q})$. The quench time $\tau_{\rm Q}$ has to be compared to the order parameter relaxation time $\tau(T)$, which for a Ginzburg-Landau system at a second order phase transition is assumed to be of the form

$$\tau(T) = \tau_0 (1 - T/T_{\rm c})^{-1} . \tag{2}$$

In superfluid ^{3}He, τ_0 is on the order of $\tau_0 \sim \xi_0/v_{\rm F}$. Here ξ_0 is the zero temperature limiting value of the temperature (T) and pressure (P) dependent superfluid coherence length $\xi(T, P)$, while $v_{\rm F}$ is the velocity of the thermal quasiparticle excitations which are excited above the superfluid energy gap. Close to $T_{\rm c}$ in the Ginzburg-Landau temperature regime, we have $\xi(T, P) = \xi_0(P)(1 - T/T_{\rm c})^{-1/2}$. Thus below $T_{\rm c}$ the order parameter coherence can be assumed to spread out with the velocity $c(T) \sim \xi/\tau = \xi_0 (1 - T/T_{\rm c})^{1/2}/\tau_0$. The freeze-out of defects occurs at time $t_{\rm Z}$, when the causally disconnected regions have grown together and superfluid coherence becomes established in the whole volume. At the corresponding freeze-out temperature $T_{\rm Z} = T(t_{\rm Z}) < T_{\rm c}$, the causal horizon has travelled the distance $\xi_{\rm H}(t_{\rm Z}) = \int_0^{t_{\rm Z}} c(T)\, dt = \xi_0 \tau_{\rm Q}(1 - T_{\rm Z}/T_{\rm c})^{3/2}/\tau_0$ which has to be equal to the coherence length $\xi(t_{\rm Z})$. This condition establishes the freeze-out temperature $T_{\rm Z}/T_{\rm c} = 1 - \sqrt{\tau_0/\tau_{\rm Q}}$ at the freeze-out time $t_{\rm Z} = \sqrt{\tau_0 \tau_{\rm Q}}$, when the domain size has reached the value

$$\xi_{\rm v} = \xi_{\rm H}(t_{\rm Z}) = \xi_0 \left(\tau_{\rm Q}/\tau_0 \right)^{1/4} . \tag{3}$$

Thus the causal horizon, behind which superfluid coherence is established, travels with the velocity

$$v_{\rm Tc} = \frac{\xi_{\rm H}(t_{\rm Z})}{t_{\rm Z}} = \frac{\xi_0}{\tau_0} \left(\frac{\tau_0}{\tau_{\rm Q}} \right)^{1/4} . \tag{4}$$

Vortex formation in neutron irradiation

Characteristic numbers for superfluid ^{3}He are $\xi_0 \sim 20$ nm, $\tau_0 \sim 1$ ns, and a quench time of $\tau_Q \sim 1$ μs. From these values we expect the domain structure to display a characteristic length scale of order $\xi_v \sim 0.1$ μm. In a U(1)-symmetry-breaking transition, vortex lines are expected to form at the domain boundaries. This leads to a network of randomly organized vortices, where the average inter-vortex distance and radius of curvature are on the order of the domain size ξ_v. In general, the KZ scaling model predicts a rapid homogeneous quench to produce a defect density (defined as vortex length per unit volume) $l_v = (a_l \xi_v^2)^{-1}$. The numerical factor $a_l \sim 1-100$ depends on the details of the model system.

2.2. Threshold velocity for vortex loop escape

The number of vortex loops which can be extracted from a heated neutron bubble depends on the applied superflow velocity v_s. More precisely, in the rotating experiments the applied flow is the counterflow velocity $\mathbf{v} = \mathbf{v}_s - \mathbf{v}_n$, where the flow velocity of the viscous normal component is $\mathbf{v}_n = \mathbf{\Omega} \times \mathbf{r}$, when the ^{3}He sample of radius R rotates at the angular velocity Ω. In fact, the neutron capture events are monitored at constant rotation Ω, so that the normal component is firmly clamped to corotate with the container. In the rotating frame of reference we then have $v_n = 0$ and $v = v_s$. The counterflow velocity v is the applied bias which determines the number of vortex loops to be extracted from the heated neutron bubble. In particular, there exists a threshold value v_{cn} for the bias, below which it will not suffice to pull vortex loops from the bubble. The dependence on the rotating counterflow bias v can be studied from the threshold v_{cn} up to the critical limit v_c at which an elemental vortex loop is spontaneously formed at the cylindrical wall in the absence of the neutron flux.[11]

Thus the threshold v_{cn} is the smallest bias velocity at which a vortex ring can escape from the heated neutron bubble. It can be connected with the size of the bubble in the following manner. A vortex ring of radius $r_\circ$ is in equilibrium in the applied counterflow at the velocity v if it satisfies the equation

$$r_\circ(v) = \frac{\kappa}{4\pi v} \ln\left(\frac{r_\circ}{\xi(T,P)}\right),\tag{5}$$

where $\kappa = 6.61 \cdot 10^{-4}$ cm^2/s is the circulation quantum. This follows from the balance between self-induced contraction and expansion by the Magnus force: a ring with a radius larger than $r_\circ$ will expand in the flow while a smaller one will contract. Thus the threshold or minimum velocity at which a vortex ring can start to expand towards a rectilinear vortex line

corresponds to the maximum possible vortex-ring size. This must be of a size comparable to the diameter of the heated bubble. For a simple estimate we set the vortex ring radius equal to that of a spherical neutron bubble: $r_{\mathrm{o}}(v_{\mathrm{cn}}) \sim R_{\mathrm{b}}$, thus $v_{\mathrm{cn}} \propto 1/R_{\mathrm{b}}$.

A simple thermal diffusion model can be used to estimate the magnitude of the radius R_{b} of the bubble which originally was heated above T_{c}. In the temperature range close to T_{c} the final phase of cooling occurs via diffusion of quasiparticle excitations out into the surrounding superfluid bath with a diffusion constant $D \approx v_{\mathrm{F}} l$, where v_{F} is their Fermi velocity and l their mean free path. For a spherically symmetric temperature profile $T(r,t)$ as a function of the radial distance r and time t, the diffusion equation is

$$\frac{\partial T(r,t)}{\partial t} = D \left(\frac{\partial^2 T}{\partial r^2} + \frac{2}{r} \frac{\partial T}{\partial r} \right) . \tag{6}$$

With the assumption that at $t = 0$ the energy E_0 is deposited at $r = 0$, the solution is given by

$$T(r,t) - T_0 \approx \frac{E_0}{C_{\mathrm{v}}} \frac{1}{(4\pi Dt)^{3/2}} \exp\left(\frac{-r^2}{4Dt} \right), \tag{7}$$

where T_0 is the temperature of the surrounding superfluid bath and C_{v} is the specific heat. The energy E_0 which is deposited as heat is close to the energy released in the nuclear reaction. (It is believed that $\sim 10\,\%$ of the reaction energy is turned into ultraviolet radiation and retarded relaxation of excited molecular complexes, ie. into components which do not contribute to the heating of the neutron bubble.) The bubble of normal fluid, $T(r) > T_{\mathrm{c}}$, expands and reaches a maximum radius

$$R_{\mathrm{b}} = \sqrt{\frac{3}{2\pi e}} \left(\frac{E_0}{C_{\mathrm{v}} T_{\mathrm{c}}} \right)^{1/3} (1 - T_0/T_{\mathrm{c}})^{-1/3} . \tag{8}$$

It then starts cooling and rapidly shrinks with the characteristic time $\tau_{\mathrm{Q}} \sim R_{\mathrm{b}}^2/D \sim 1\mu$s. Since v_{cn} is inversely proportional to R_{b}, it has the temperature dependence $v_{\mathrm{cn}} \propto (1 - T_0/T_{\mathrm{c}})^{1/3}$ close to T_{c}. Also, the prefactor of Eq. (8) decreases with increasing pressure as both C_{v} and T_{c} grow. Thus v_{cn} should increase with pressure. These predictions for the temperature and pressure dependences of v_{cn} agree semi-quantitatively with measurements.[2,6]

2.3. Escape rate of vortex loops

During the quench-cooling of the neutron bubble through the superfluid transition, a random vortex network is formed within the bubble.[4] According to the KZ model,[4] the characteristic length scale of the network (i.e.

Vortex formation in neutron irradiation

the average inter-vortex distance and average radius of curvatures of the vortices) is comparable to the order parameter inhomogeneity ξ_v, which is precipitated in the quench. The later evolution of the network leads to a gradual increase in this length. We shall call this time-dependent length $\tilde{\xi}(t)$. In the following we assume that this "coarse-graining" process of the network preserves its random character, in other words the network remains self similar or scale invariant. Only later a change occurs in this respect, when the loops become sufficiently large to interact with the externally applied bias field: This causes large loops with a radius exceeding the critical value from Eq. (5) to expand, if they are oriented transverse to the flow with the correct winding direction. Eventually such loops are extracted to the bulk and grow to become rectilinear vortex lines in the center of the sample. (At high temperatures in the absence of turbulence the number of vortices is conserved, after the evolution of the random network is finished and well-defined loops in the bulk bias field have been formed.) The small loops in the network contract and disappear. The time scale of these processes is determined by the mutual friction damping between the normal and superfluid components. In the high temperature range the evolution of the vortex network occurs in milliseconds and the growth of the extracted vortex rings into rectilinear lines happens in a fraction of a second.

The number of vortex loops, which are extracted from the network and are observed in the measurement, can be found from the following considerations. The energy of a vortex loop, which is stationary with respect to the walls, is given by[12]

$$\mathcal{E} = E_{\mathrm{kin}} + \mathbf{p}\mathbf{v} , \tag{9}$$

where $\mathbf{v}$ is the velocity of the bias flow. The hydrodynamic kinetic energy or self-energy of the loop arises from the trapped superfluid circulation with the velocity $v_{\mathrm{s,vort}}$,

$$E_{\mathrm{kin}} = \frac{1}{2} \int \rho_{\mathrm{s}} v_{\mathrm{s,vort}}^2 \, dV = \varepsilon L , \tag{10}$$

and is proportional to the length L of the loop and its line tension,

$$\varepsilon = \frac{\rho_{\mathrm{s}} \kappa^2}{4\pi} \ln \frac{\tilde{\xi}(t)}{\xi} . \tag{11}$$

Here we neglect the small contribution from the core energy, use $\tilde{\xi}(t)$ for the diameter of the loop, and the superfluid coherence length $\xi(T, P)$ for the diameter of the core. This equation is valid in the logarithmic approximation, when $\tilde{\xi}(t) \gg \xi(T, P)$. While the first term in Eq. (9) is proportional to the length L of the loop, the second term involves its linear momentum,

$$\mathbf{p} = \int \rho_{\mathrm{s}} \mathbf{v}_{\mathrm{s,vort}} \, dV = \frac{1}{2\pi} \rho_{\mathrm{s}} \kappa \int \nabla \Phi \, dV = \rho_{\mathrm{s}} \kappa \mathbf{S} , \tag{12}$$

where the last step follows from Gauss's theorem and involves the area S of the loop in the direction of the normal $\mathbf{S}/S$ to the plane of the loop. Thus we write for the energy of a loop

$$\mathcal{E}(L, S, t) = \rho_{\mathrm{s}}\kappa \left[L \, \frac{\kappa}{4\pi} \, \ln\frac{\tilde{\xi}(t)}{\xi} \; - \; vS \right] \; , \tag{13}$$

where S is now the algebraic area perpendicular to the flow and of proper winding direction. This equation expresses the balance between a contracting loop due to its own line tension, which dominates at small bias velocities, and expansion by the Magnus force from the superflow, which dominates at high bias velocities. The divide is the equilibrium condition, which was expressed by Eq. (5) and corresponds to the situation when the height of the energy barrier, which resists loop expansion, vanishes. In this configuration $\mathbf{p}$ is antiparallel to $\mathbf{v}$, the loop moves with the velocity $-\mathbf{v}$ in a frame of the superfluid component, but is stationary in the rotating frame.

The expansion of the vortex loop should be calculated by including the mutual friction forces. In our analytic description of vortex loop escape we shall neglect such complexity. Instead we shall make use of three scaling relations which apply to Brownian networks[13] and are derived from simulation calculations described in Ref. 10. These expressions relate the mean values in the statistical distributions of the loop diameter $\mathcal{D}$, area S, and density n to the length L of the loop:

$$\mathcal{D} = AL^{\delta}\,\tilde{\xi}^{1-\delta} \; , \quad (A \approx 0.93, \; \delta \approx 0.47) \; , \tag{14}$$

$$|S| = B\mathcal{D}^{2-\zeta}\,\tilde{\xi}^{\zeta}, \quad (B \approx 0.14, \; \zeta \approx 0) \; , \tag{15}$$

$$n = CL^{-\beta}\,\tilde{\xi}^{\beta-3} \; , \quad (C \approx 0.29, \; \beta \approx 2.3) \; . \tag{16}$$

For a Brownian random walk in infinite space the values of δ, β and ζ are $1/2$, $5/2$ and 0. The important assumption is that these relations are valid during the entire evolution of the network, until sufficiently large rings are extracted by the counterflow into the bulk. Using Eqs. (14) and (15), we may write Eq. (13) for the energy of a loop in the form

$$\mathcal{E}(\mathcal{D}, t) = \rho_{\mathrm{s}}\kappa\mathcal{D}^2 \left[\frac{\kappa}{4\pi\tilde{\xi}(t)A^2} \, \ln\frac{\tilde{\xi}(t)}{\xi} \; - \; vB \right] \; . \tag{17}$$

When the mean diameter $\tilde{\xi}(t)$ exceeds a critical size $\tilde{\xi}_{\mathrm{c}}(v)$, which depends on the particular value of the bias velocity v,

$$\tilde{\xi}_{\mathrm{c}}(v) = \frac{1}{A^2 B} \, \frac{\kappa}{4\pi v} \, \ln\frac{\tilde{\xi}_{\mathrm{c}}}{\xi} \; , \tag{18}$$

Vortex formation in neutron irradiation

the energy in Eq. (17) becomes negative and the loop starts expanding spontaneously. This is the smallest loop which will be able to expand at a given value v. The upper cutoff for the loop size distribution is provided by the diameter of the entire network, or that of the heated bubble, $2R_b$, such that $\tilde{\xi}_c(v_{cn}) = 2R_b$. The total number of loops N_b, which will be extracted from one neutron bubble, can then be obtained from

$$N_b = V_b \int_{\tilde{\xi}_c}^{2R_b} d\mathcal{D} \; n(\mathcal{D}) \; . \tag{19}$$

Here the density distribution $n(L) = C \; \tilde{\xi}^{-3/2} \; L^{-5/2}$, combined with that for the average diameter $\mathcal{D}(L) = A \; (L \; \tilde{\xi} \;)^{1/2}$, gives $n(\mathcal{D}) \, d\mathcal{D} = 2A^3 C \mathcal{D}^{-4} \, d\mathcal{D}$. On inserting this into the integral (19) we obtain

$$N_b = \frac{1}{9}\pi A^3 C \left[\left(\frac{2R_b}{\tilde{\xi}_c} \right)^3 - 1 \right] \; . \tag{20}$$

From this equation we see that the requirement $N_b(v_{cn}) = 0$ returns us the definition of the threshold velocity v_{cn}: $\tilde{\xi}_c(v = v_{cn}) = 2R_b$. This in turn gives us from Eq. (18) for the radius of the heated bubble

$$R_b = \frac{1}{A^2 B} \; \frac{\kappa}{8\pi v_{cn}} \; \ln \frac{2R_b}{\xi(T,P)} \tag{21}$$

Eqs. (18) and (21) show that $\tilde{\xi}_c \propto 1/v$ and $R_b \propto 1/v_{cn}$, so that we may write for the vortex-formation rate $\dot{N} = \phi_n N_b$ from Eq. (20)

$$\dot{N} = \frac{1}{9}\pi A^3 C \phi_n \left[\left(\frac{v}{v_{cn}} \right)^3 - 1 \right] \; , \tag{22}$$

where ϕ_n is the neutron flux. Thus the rate, at which vortex loops are extracted into the bias flow under neutron irradiation, has a cubic dependence on the bias velocity v and reflects the dependence on the volume of the heated neutron bubble. By inserting $A \approx 0.93$, $C \approx 0.29$ from Eqs. (14) and (16), respectively, and $\phi_n \approx 20$ neutrons/min (as appropriate for the saturation of the event rate $\dot{N}_e$ in the center panel of Fig. 2), we obtain for the prefactor in Eq. (22) $\gamma = \frac{1}{9}\pi A^3 C \phi_n \approx 1.6$ min^{-1}. We may also define a threshold velocity v_{cni} for an event in which i loops are formed simultaneously, using the approximate requirement $N_b(v = v_{cni}) \approx i$. This gives $v_{cni}/v_{cn} \sim i^{1/3}$. These results are found to be consistent with measurements.

2.4. Non-uniform thermally driven transition

The cubic dependence on the bias flow in Eq. (22) comes from the assumption that the whole volume of the heated bubble contributes equally to the production of vortex loops. In the rapidly cooling neutron bubble there is a steep thermal gradient such that the causal horizon, behind which superfluid coherence is established, lags behind the temperature front, where T drops below T_c. To characterize such a non-uniform quench,[14] we need in addition to the quench time τ_Q a second parameter, the thermal length scale $\lambda = [|\nabla T|/T_c]^{-1}$. The temperature front can then be assigned a velocity of order $v_T \sim \lambda/\tau_Q$. If the transition is slow, the causal horizon will keep abreast of the thermal front and superfluid coherence will not be broken. However, in a rapid non-equilibrium situation $v_T > v_{Tc}$ and the KZ mechanism will survive in the space between the two separated fronts.

In the case of the heated neutron bubble $\lambda \sim R_b \sim 50\,\mu\text{m}$ and so $v_T \sim 50\,\text{m/s}$, which is of the same order of magnitude as v_{Tc} from Eq. (4). Thus we do not expect a serious suppression in vortex formation owing to the nonuniformity of the temperature distribution.

2.5. Alternative explanations of vortex formation

The neutron-capture experiment in rotating ^{3}He-B is not an exact replica of the ideal KZ model, a quench-cooled second order transition in an infinite homogeneous medium. In the neutron bubble there is a strong thermal gradient and a strict boundary condition applies at its exterior, imposed by the bulk superfluid state outside. The cool-down occurs so fast that any extrapolation from the equilibrium state theories is uncertain, whether it concerns the hydrodynamics or the superfluid state. Non-equilibrium phase transitions are notoriously a complicated issue and any interpretation has to be questioned. Nevertheless, the predictions of the KZ model, as summarized above, are semi-quantitatively supported by the experimental observations.[10] One may still argue whether this fact constitutes final proof or not: Perhaps other processes can be found which also explain the experimental observations?

Besides the KZ mechanism, the only alternative model which at the moment exists on the level of quantitative predictions is a surface instability – the production of vortex rings around the circumference of the heated neutron bubble, at the interface between the surrounding cold superfluid bath and the hot normal liquid in the center. This model was worked out by Aranson *et al.* (Ref. 15). They demonstrated that the moving normal-superfluid interface becomes unstable in the presence of the superflow along

the interface. Numerical simulations show that the outcome of this instability is the production of vortex rings which encircle the bubble and are perpendicular to the applied flow. These rings screen the superflow, so that the superfluid velocity (in the rotating frame) is zero inside the bubble.

It is obvious that the possible influence of the surface instability has to be examined carefully: During the cooling the fluid in the shell around the normal bubble still remains in the B phase but is heated above the surrounding bulk temperature T_0. In the Ginzburg-Landau temperature regime the intrinsic instability velocity $v_{cb}(T, P)$ of the bulk superfluid decreases with increasing temperature.[11] If no other process intervenes, the superflow instability therefore necessarily has to occur within that peripheral warm shell surrounding the hot neutron bubble, where the local temperature corresponds to the temperature at which the bias velocity v equals the critical value $v_{cb}(T, P)$ for bulk superflow.

After their formation, the rings, which are produced by the surface instability, start to expand and will eventually be pulled away by the Magnus force. It is thus conceivable that these rings might give rise to the rectilinear vortex lines which are observed in the NMR measurements. How do we distinguish from the measured data whether the surface instability or the KZ mechanism is responsible for the observed vortex lines? The critical velocity v_{cn} does not discriminate between the two processes. In both cases it is determined by the stability velocity (Eq. (5)) for the largest vortex ring which fits the bubble. However, the different nature of the two processes has important consequences for the vortex formation rate.

The row of vortex rings, which is produced by the surface instability to screen the neutron bubble, resembles a vortex sheet between the superfluid, moving with velocity v outside the bubble, and the stationary superfluid inside. The density of vorticity in the sheet is v/κ and the number of loops produced by one neutron absorption event is $N_b \propto vR_b/\kappa$, where R_b is the size of the bubble along the flow direction. Thus N_b grows linearly with the applied flow velocity. This estimate is supported by the numerical simulations.[15] In contrast, the KZ mechanism is a volume effect, which results in the cubic dependence expressed in Eq. (22). This is a major distinguishing feature between the two mechanisms, from the experimental point of view.

In addition, the surface instability should be a deterministic process which in every event produces the same surface density of vortex rings. Variations in the number of rings arises only owing to variations in the shape of the neutron bubble and its orientation with respect to the bias flow. (Unfortunately, the distribution of the number of rings was not studied in detail in the simulations.[15]) In contrast, the KZ mechanism produces a

random vortex network. The number of loops which is extracted by the applied flow from such a network is inherently a stochastic number with a relatively wide distribution.

Finally, the surface instability is not particularly sensitive to the processes inside the heated neutron bubble. Only regular mass-flow vortices are expected to form. The KZ mechanism, on the other hand, can be expected to produce all possible different kinds of defects. Their presence might be either directly observed in the final state or via their influence on the evolution of the vortex network inside the neutron bubble.

All these features can be checked in the experiment. As outlined in the next paragraph, the experimental results are undoubtedly more consistent with the KZ mechanism. This fact is puzzling: From the two processes the surface instability should be the dominant one. As long as the rings created by the surface instability encircle the neutron bubble, they shield its central volume from the bias flow and any vorticity within the bubble – which might have been created by the KZ mechanism – will collapse in the presence of dissipation. This is exactly what was seen in the numerical simulations[15] with a rapidly cooling model system represented by a scalar order parameter. The thermal diffusion equation was used to account for the cooling and the order-parameter relaxation was obtained from the time-dependent Ginzburg-Landau equation. It was then found that both processes give rise to vortex formation, but the rings, which eventually manage to escape into the bulk, originate from the bubble boundary.

The discrepancy between simulation and experiment demonstrates that the competition between the two vortex formation mechanisms is not as straightforward as described above. Possibly in the conditions of the experiment the surface instability develops so slowly that the random KZ network manages to form earlier. The polarization of the network by the bias flow might then stop the development of the surface instability. Also the diffusion model, which is used both here in Sec. 2.2. and in Ref. 15 for the cooling of the bubble, is a gross oversimplification.[16] This fact might be another important source for the discrepancy.

2.6.   Comparison with experiment

The dependence of the formation rate $\dot{N}$ of rectilinear vortex lines on the externally applied bias velocity $v = |\mathbf{v}_s - \mathbf{v}_n|_{r=R} = \Omega R - \kappa N/(2\pi R)$ is the central quantitative result from the rotating measurements. It is most efficiently measured close to T_c where the resolution in NMR absorption is sufficient to resolve individually the rectilinear vortex lines which are formed

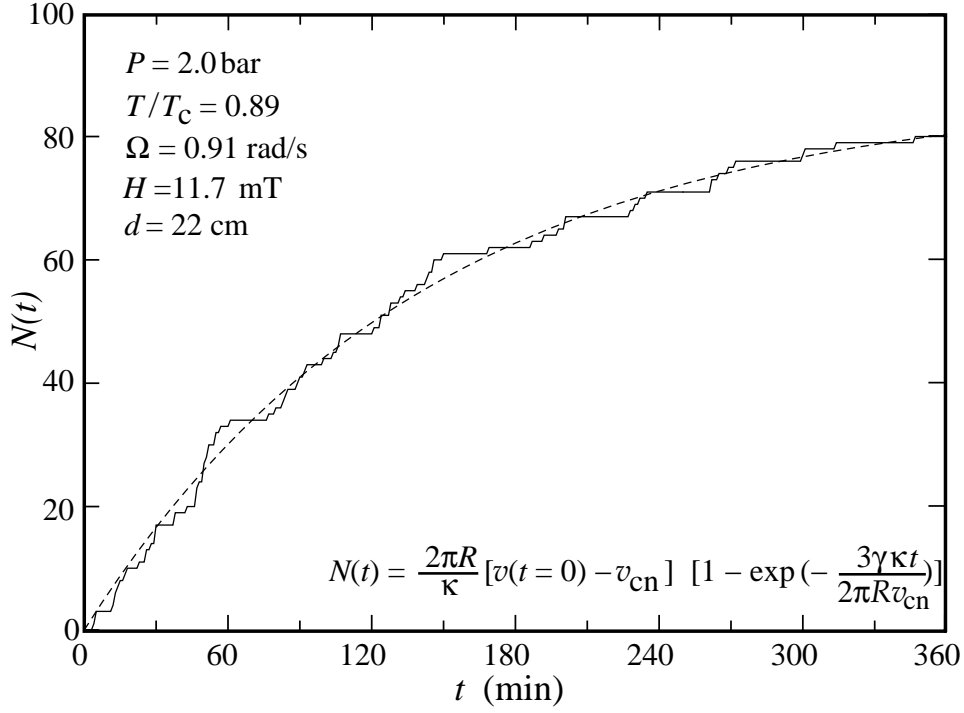**Vortex formation in neutron irradiation**

Fig. 1. Measurement of vortex formation in neutron irradiation at high temperatures. Each discontinuous step in the measured staircase trace corresponds to a different neutron absorption event. The height of the step gives the yield of rectilinear vortex lines from this event. At $t = 0$ the neutron irradiation is turned on at constant flux on the initially vortex-free ^{3}He-B sample rotating at constant Ω. The dashed curve represents the expression shown in the panel which has been integrated from the rate Eq. (22). The values of the two parameters, $\gamma = 1.1$ min^{-1} and $v_{cn} = 1.9$ mm/s, have been chosen to give a good fit, but agree within the measuring accuracies with all other measurements in the temperature range from T_c down to $0.80\,T_c$. The data in Figs. 2 and 3 have been collected by measuring the initial slope of this curve, $\dot{N}(t)$ at $t = 0$.

in each neutron capture event.

Fig. 1 illustrates a measurement where the cumulative number of vortex lines $N(t)$ has been recorded as a function of time t over a period of 6 hours.[17] Initially, when the neutron flux is turned on, the sample is rotating at constant angular velocity in the vortex-free state. First the vortex formation rate $\dot{N}$ is high and individual neutron absorption events produce several rectilinear vortex lines. The lines accumulate in a dense cluster which lies coaxially in the center of the cylindrical sample. As the number of lines in

the cluster N grows, the bias velocity v is reduced. Consequently the rate $\dot{N}$ decreases gradually with time and finally at some critical value of the bias $v = v_{cn}$ vortex formation stops altogether. The measurement illustrates that in constant conditions the vortex formation rate $\dot{N}$ is indeed controlled by the bias velocity v and not by the velocity of the normal component $v_n(R) = \Omega R$, which is constant during this entire measurement. The dashed curve through the data is fully specified by the two parameters, the rate parameter γ, which is a constant for a given measuring setup with fixed neutron flux, and the threshold velocity v_{cn}, which contains the dependence on the sample variables (temperature, pressure, magnetic field). The large excursions of the measured data from the dashed curve illustrate the stochastic nature of the accumulation process.

The three panels in Fig. 2 describe in more detail the comparison of the rate equation (22) to measurements.[6] From the staircase like NMR absorption, as shown in Fig. 1, one counts both the escape rate for vortex loops and the frequency of successful neutron capture events, *ie.* the events which lead to vortex-line formation. This requires a weak thermal neutron flux so that two neutron capture events do not overlap in time. In the measurements the rate was adjusted by changing the distance d between the paraffin-moderated Am-Be neutron source and the ^{3}He sample.[10] The three rates in Fig. 2 have been determined independently and directly by counting the number of rectilinear vortex lines from each measured event separately. To construct the plot, the horizontal axis was divided into equal bins from which all individual measurements were averaged to yield the evenly distributed data points displayed in the panels. The rates increase rapidly with the bias velocity v from the critical threshold v_{cn} to $4.5\,v_{cn}$. This upper limit is close to the maximum possible bias velocity, imposed by the spontaneous instability limit of this particular sample container.

The top panel in Fig. 2 demonstrates the cubic dependence of the vortex formation rate $\dot{N}$ on the bias flow. A linear dependence would here fall outside the experimental uncertainty limits. Also note that in agreement with the scaling properties of the rate equation (22), measurements at the two pressures of 2 and 18 bar fall on the same universal curve as a function of v/v_{cn}.

The center panel illustrates the rate of those neutron absorption events $\dot{N}_e$ which produce at least one line and thus become observable in the NMR absorption measurement (i.e. produce a step of any size in Fig. 1). This plot shows that the rate of successful events increases with bias flow and appears to saturate at about 20 neutrons/min. This is the flux of neutrons absorbed in the sample, as also estimated from independent measurements with commercial monitoring devices for thermal neutrons.[10] The measure-
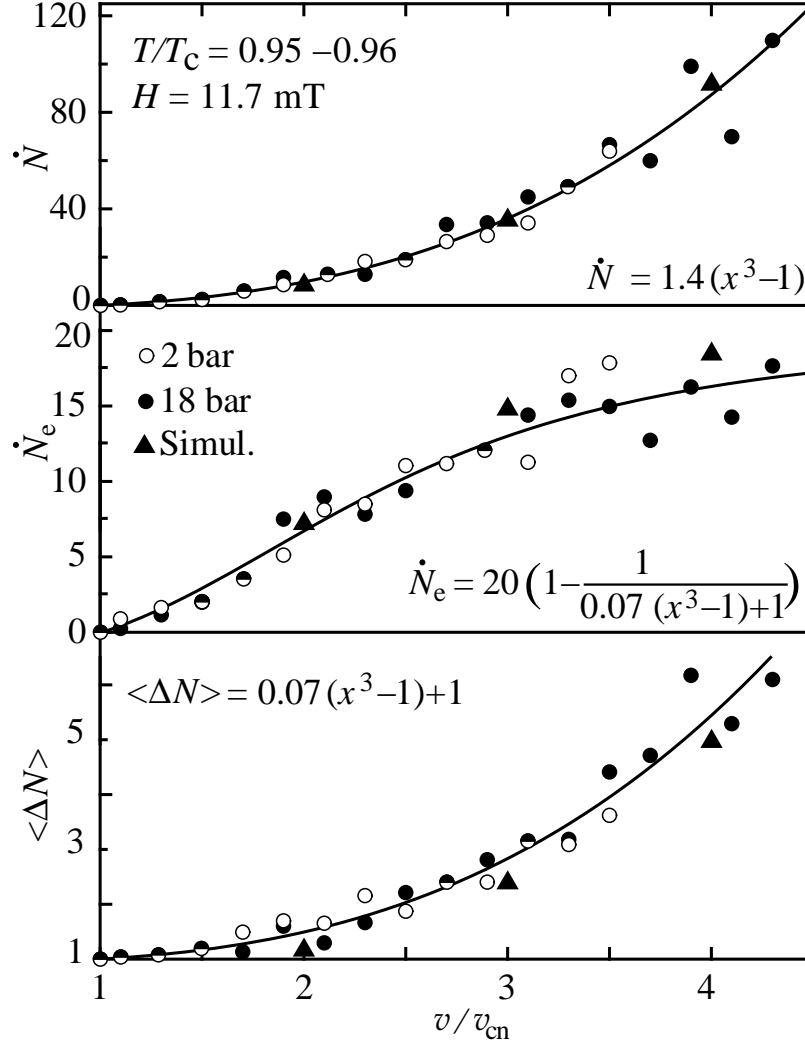
Fig. 2. Different rates in neutron-induced vortex formation, plotted *vs* normalized bias flow velocity v/v_{cn}: *(Top)* the total number of rectilinear lines $\dot{N}$ formed per minute, *(middle)* the number of observed neutron absorption events $\dot{N}_e$ per minute, and *(bottom)* the average number of lines $\langle \Delta N \rangle$ formed per observed event. All three rates have been counted *independently* from discontinuities in NMR absorption with single-vortex amplitude resolution and single-event time resolution. The two upper plots correspond to an incident neutron flux of about 20 neutrons/min. The bottom plot is neutron-flux independent. The solid curves are fits to the data, given by the expressions in each panel. Triangles are results of numerical simulations described in Ref. 10.

ment thus involves a strong stochastic element – close to the critical threshold at $v = 1.1v_{\mathrm{cn}}$ only one neutron capture event from 40 manages to produce a sufficiently large vortex loop for spontaneous expansion. On increasing the bias flow by a factor of four, almost all neutron capture events give rise to at least one escaping vortex loop.

The bottom panel records the average number of vortex loops $\langle \Delta N \rangle$ which are extracted from each detected neutron absorption event (i.e. the average height of the step in Fig. 1). Considering all three panels of Fig. 2, we now realize that the rapid increase of $\dot{N}$ as a function of v/v_{cn} arises from the increase in both the event rate $\dot{N}_{\mathrm{e}}$ and the number of lines produced per event $\langle \Delta N \rangle$. This conclusion fits with the KZ predictions, while for the surface instability one would expect $\dot{N}_{\mathrm{e}}(v)$ to resemble a step function and $\langle \Delta N \rangle$ to increase linearly with v.

The most detailed information from the rate measurements is the dispersion into events in which a given number of rectilinear lines ΔN is formed.[6] Fig. 3 displays the distribution of the observed events as a function of ΔN, at different values of the bias flow. This result is the clearest demonstration for the stochastic nature of the vortex formation process: The width of each distribution is comparable to its average value $\langle \Delta N \rangle$. Such a distribution can hardly be expected to result from the deterministic surface instability. However, as shown in the figure, the distributions can be reproduced without any fitting parameters with numerical simulations of the evolution of a vortex network in the bias flow, if the network is completely random and has the of proper initial spatial extension.[10]

The superflow instability at the periphery of the neutron bubble should not be sensitive to the processes in the hot interior. Therefore another link to the KZ model would be the identification of any signatures from the primordial disorder in the order parameter distribution which was originally precipitated during the quench cooling. Several observations point to such evidence. One of these is the fact[7] that the spin-mass vortex is formed in the neutron absorption process at high bias flow, when $v/v_{\mathrm{cn}} \gtrsim 2$. The spin-mass vortex is a combined defect. It consists of a usual mass-flow vortex (resulting from broken $U(1)$ symmetry) embedded within a domain-wall-like soliton (resulting from broken relative $SO(3)$ symmetry in the rotation of the spin and orbital coordinate systems with respect to each other). It is difficult to explain the formation of this composite in the context of a flow instability, since mass flow does not interact directly with the spin of the order parameter. In contrast, fluctuations in a non-equilibrium transition could be expected to produce different types of inhomogeneity in a multi-component order parameter distribution.

The same argument holds for the competition between A and B phase
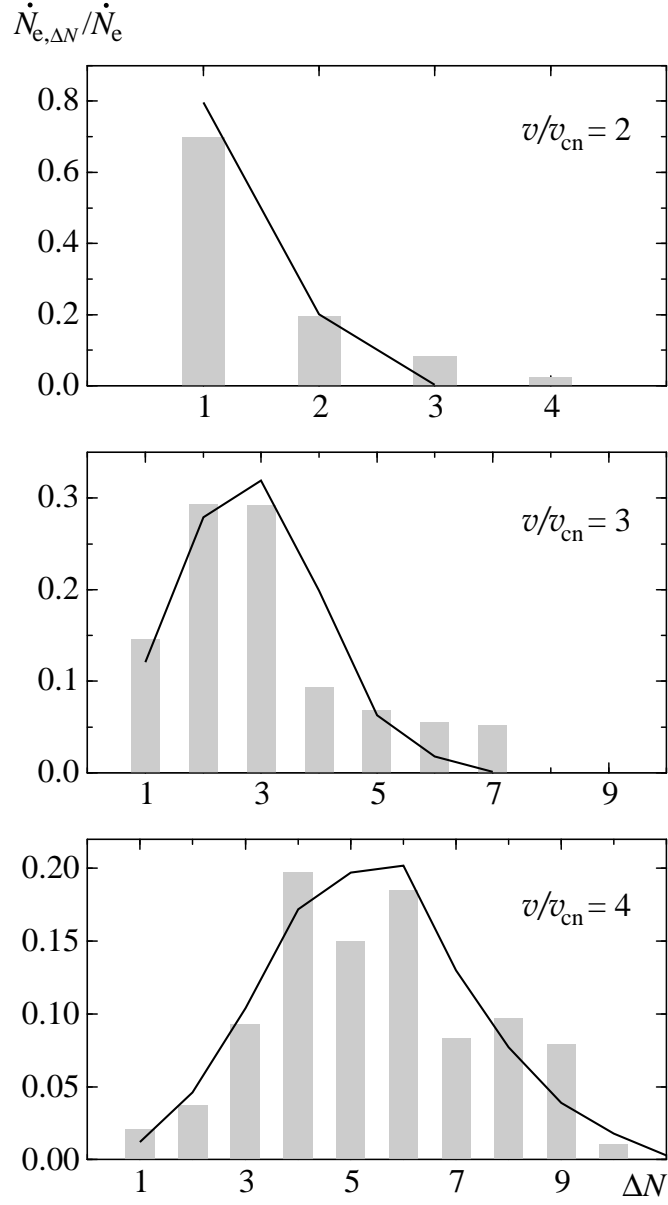
Vortex formation in neutron irradiation

Fig. 3. Distribution of neutron-induced vortex formation events, as a function of the number of rectilinear vortex lines ΔN produced in a single event at different values of the bias flow v (normalized to the critical velocity v_{cn}). The rate of events $\dot{N}_{e,\Delta N}$ producing the specific number of lines ΔN, normalized to the total event rate $\dot{N}_e$, is shown. The vertical bars represent the experimental data (at $P = 2\,\text{bar}$, $T = 0.96\,T_c$, and $H = 11.7\,\text{mT}$). The lines are from the simulation calculations described in Ref. 10.

.

order-parameter components as a function of pressure or magnetic field. Measurements show[6] that there is an abrupt increase in v_{cn} and a corresponding reduction in the vortex formation rate $\dot{N}(v)$, when the pressure is increased above the polycritical point in the superfluid ^{3}He phase diagram. The increase in v_{cn} is larger than one would expect from the decrease of the bubble size with pressure, according to Eq. (8). In this pressure regime a sliver of stable A phase exists below T_c in the equilibrium phase diagram. The measurement is performed at a bath temperature T_0 which corresponds to the stable B-phase regime, but in the quench cooling process the existence of the A-phase sliver can be expected to interfere. Thus the observed reduction in $\dot{N}$ has been interpreted to indicate that with increasing pressure larger regions of the primordial order parameter distribution after the rapid cool-down of the neutron bubble are occupied by A-phase seeds which do not contribute to the formation of the B-phase vortex network.[18] In this way the available volume for the B-phase network is reduced. The preference of order parameter fluctuations to promote A-phase components with increasing pressure has been discussed by Bunkov *et al.* in the context of non-equilibrium transitions.[19] Similarly with increasing magnetic field the fluctuations are likely to be biased more and more towards the A-phase regime of the order parameter space.

The presence of the A-phase connected pressure and magnetic field dependences have been established in measurements,[6] but more details of these features should be worked out. These phenomena are believed to be related to the observation[20] that in supercooled A phase a transition to B phase can be triggered by a neutron absorption event, while no transitions are observed in the absence of the neutron flux. The current view holds that in supercooled A phase homogeneous B-phase nucleation is impossible,[16] but that extrinsic effects, of which only ionizing radiation has been clearly identified so far, become responsible for the A→B transitions which in practice are always eventually seen when the temperature is reduced.

3.   VORTEX FORMATION BELOW $0.6\,T_c$

The measurements of neutron-induced vortex formation in rotating ^{3}He-B were formerly not extended below $0.80\,T_c$ because of resolution difficulties: In the B phase, the susceptibility drops with decreasing temperature, while the width of the NMR spectrum increases. Thus the change of NMR absorption per one rectilinear vortex line quickly diminishes and single-vortex resolution is lost. Recently a new phenomenon was discovered:[25] If a few seed vortex loops are injected into rotating vortex-free superflow in the B

phase at temperatures $< 0.6\,T_\mathrm{c}$, they become easily unstable and form a turbulent vortex tangle. In the turbulent state the number of vortices rapidly multiplies and the final state is an equilibrium array of rectilinear lines. The change from vortex-free to equilibrium rotation is easy to detect with NMR at all temperatures! Neutron irradiation provides a convenient, almost temperature-independent way to inject locally into the flow vortex loops. Their number can be tuned in the range 1–5 by choosing the bias velocity (see Fig. 3). Thus it became instructive to study the transition to turbulence when the seed loops are provided by a neutron absorption event. Below we examine this transition and present therefore results on both regular and turbulent vortex formation in neutron irradiation at temperatures $0.4 < T/T_\mathrm{c} < 0.6$.

3.1.   Experimental techniques

Our measurements are performed in the setup[21] shown in Fig. 4. For the study of turbulence it proved fortunate that this arrangement includes two NMR detection coils at both ends of the long sample cylinder. A second bonus was the relatively high critical velocity of the container so that vortex-free superflow could be maintained to high rotation velocities. The sample cylinder was prepared from quartz glass by fusing the two flat end plates with two sections of tubing under an acetylene flame. Subsequently the finished glass structure was annealed in an oven, carefully cleaned with solvents, and mildly etched with dilute HF.

Experience shows that on an average sample containers with such surfaces display relatively high critical velocities and low trapping of remanent vortices. However, the exact critical velocity of a sample container is a property which is not in good control: Presumably one bad spot on the cylindrical surface or even a loose dirt particle may spoil the result. A number of similar containers have been used with sizeable variation in their critical properties. In one case it was observed that the critical velocity dropped by $50\,\%$ in the middle of the experiment, after reducing the pressure from 34 to 29 bar, presumably because of a dislodged dirt particle. The latest sample tube, with which the data in this report were collected, had a critical velocity which was above $3.5\,\mathrm{rad/s}$ (which is the safe upper rotation limit of our cryostat) below $0.8\,T_\mathrm{c}$ at 29.0 bar.

The lower section of the ^{3}He volume below the orifice is directly connected with the sintered heat exchanger. This section is flooded with remanent vortices from the porous sinter already at low rotation. Generally we find that vortices leak more and more through the orifice into the sample
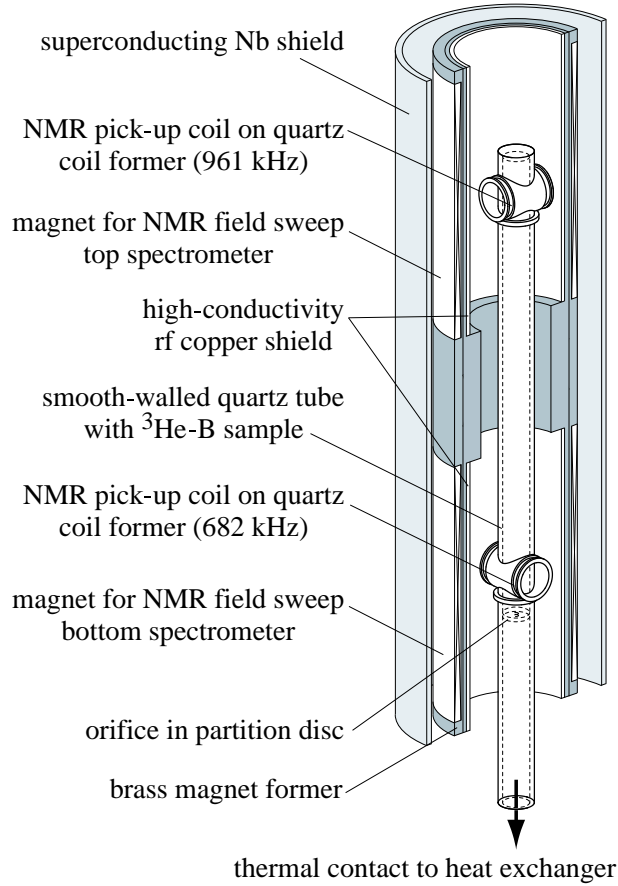
superconducting Nb shield

NMR pick-up coil on quartz
coil former (961 kHz)

magnet for NMR field sweep
top spectrometer

high-conductivity
rf copper shield

smooth-walled quartz tube
with ^{3}He-B sample

NMR pick-up coil on quartz
coil former (682 kHz)

magnet for NMR field sweep
bottom spectrometer

orifice in partition disc

brass magnet former

thermal contact to heat exchanger

Fig. 4. ^{3}He sample with NMR measuring setup.[21] The sample is contained in a fused quartz glass tube which has a diameter of 6 mm and length 110 mm. This space is separated from the rest of the liquid ^{3}He volume with a partition disc. In the disc an orifice of 0.75 mm diameter provides the thermal contact to the liquid column which connects to the sintered heat exchanger on the nuclear cooling stage. Two superconducting solenoidal coil systems with end-compensation sections produce two independent homogeneous field regions with axially oriented magnetic fields. An exterior niobium cylinder provides shielding from external fields and additional homogenization of the NMR fields. The NMR magnets and the Nb shield are thermally connected to the mixing chamber of the pre-cooling dilution refrigerator and have no solid connection to the sample container in the center. The two split-half detection coils are fixed directly on the sample container, are wound from superconducting copper-nickel clad multi-filamentary wire of 0.05 mm diameter, and have two layers of windings (2×26 turns) in each half. To minimize rf losses high conductivity copper shields are installed inside the bores of the magnets.

volume on cooling below $0.6\,T_c$. Surprisingly the sample tube, with which the present measurements were performed, was immune to this problem in spite of the fact that the orifice had a relatively large diameter of $0.75\,$mm. Thus in this sample container vortex formation in neutron irradiation can be studied up to $3.5\,$rad/s above $0.40\,T_c$ if care is exercised to avoid weakly trapped remanent vortices.[22] It was noted that at low temperatures successive accelerations to rotation have to be separated by extensive waiting periods at stand still, to allow remanent vortices to slowly annihilate. Just below $0.60\,T_c$ this waiting time proved to be around $5\,$min, but at $0.40\,T_c$ it was found to be of order $30\,$min. Otherwise vortex-free rotation at velocities above $1\,$rad/s was not possible to achieve.

The sample tube is filled and pressurized with liquid ^{3}He while the nuclear cooling stage is maintained at temperatures below $0.15\,$K. In this way a new sample can be cooled to the lowest temperatures in one week, in spite of the large thermal resistance of the long liquid ^{3}He column and the orifice. In the superfluid temperature range the thermal response of the sample cylinder is fast, the thermal gradient along the column is small, and the sample was cooled to $0.3\,T_c$ at pressures above $10\,$bar.

The experimental setup is equipped with two independent continuous-wave NMR spectrometers. Each spectrometer includes a split-half excitation/detection coil. The two coils are installed at both ends of the sample cylinder. Each coil is part of a high-Q tank circuit. For the upper coil the resonance frequency of the tank circuit is $961.2\,$kHz and the Q-value 10800. The tank circuit with the lower coil is tuned to $681.8\,$kHz and has a Q of 8800. Each spectrometer operates as a Q meter and is equipped with a GaAs MESFET preamplifier, which is cooled to liquid He temperature and is followed by room-temperature phase-locked detection. Fig. 5 shows a number of absorption spectra measured with the bottom spectrometer. The spectra illustrate the relevant NMR line shapes which one encounters with varying numbers of rectilinear vortex lines in the sample. To obtain reproducible line shapes the sample needs to be accelerated to high rotation and in different rotation directions, while still at high temperatures around $0.8\,T_c$. This homogenization procedure improves the order parameter texture by displacing solitons and other defects from the sample volume.

Three spectra in Fig. 5 have a sharp maximum on the left which arises from the vortex-free bias flow. It is traditionally called the *counterflow* (CF) peak. If vortices are formed, these accumulate as rectilinear lines in a central vortex cluster. The superflow outside the cluster is then reduced and both the height and total intensity of the CF peak drop. The reduction is proportional to the number of new rectilinear vortex lines if the overall change from the vortex-free state remains sufficiently small. In contrast,
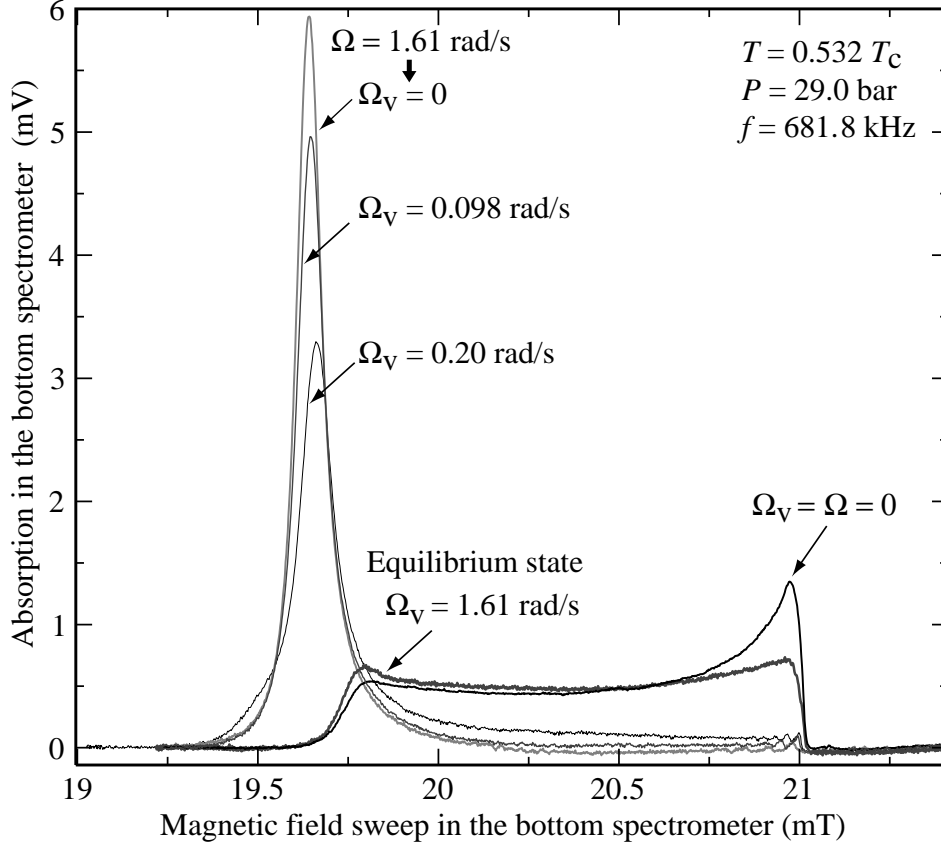
Fig. 5. NMR absorption spectra of ^{3}He-B in rotation. With large vortex-free superflow the shape of the spectrum is a sensitive function of the number of vortex lines N. Here N is characterized by the rotation velocity $\Omega_v(N)$ at which a given number of lines N is in the equilibrium state. The different spectra have been measured with the RF excitation at constant frequency f, using a linear sweep of the axially oriented polarization field H. The spectra have been recorded at constant temperature and thus all have the same integrated total absorption. The sharp absorption maximum at low field is called the *counterflow peak* (CF). Its shift from the Larmor field (at $21.02\,\mathrm{mT}$) is used for temperature measurement. When a central cluster of rectilinear vortex lines is formed, the height of the CF peak is reduced. In the *equilibrium vortex state* ($\Omega = \Omega_v$), where the number of vortex lines reaches its maximum, the spectrum looks very different: it has appreciable absorption at high fields and borders prominently to the Larmor edge. This spectrum is more similar to that of the *non-rotating state* ($\Omega = 0$). As shown in Fig. 6, when the vortex number is small, $\Omega_v \ll \Omega$, the reduction in the CF peak height can be conveniently calibrated to give Ω_v and thus N.

the line shape looks very different in the equilibrium rotating state, when the entire sample is filled with rectilinear lines and the large-scale vortex-free superflow is practically absent. As a function of vortex number N, the change from the vortex-free to the equilibrium spectrum is by no means linear at constant Ω. In fact close to the equilibrium state $(\Omega - \Omega_{\mathrm{v}}(N) \lesssim 0.2 \, \mathrm{rad/s})$, the spectrum is already almost insensitive to any changes in N. Here we denote with $\Omega_{\mathrm{v}}(N)$ the rotation velocity at which a given number of vortex lines N is in equilibrium rotation. Therefore in the general case, to determine N one has to increase rotation to some reference value where the sensitivity of the CF peak is restored.[11] This requires that the textures are stable and reproducible and that new vortices are not formed during rotational acceleration. In the neutron irradiation measurements below we primarily need to distinguish two cases from each other, the production of a small number of rectilinear vortex lines or the equilibrium number after a turbulent event. As seen from Fig. 5, this task can be accomplished just by inspection of the spectra without any calibration.

For measurements of the vortex formation rate in non-turbulent conditions a calibration of the CF peak height with respect to the number of vortex lines is required. Fig. 6 shows an example of a such calibration. The measurement was performed for small vortex clusters $(N \lesssim 100)$ using the following procedure: A vortex cluster of given size is formed and measured in a four step process. 1) First the spectrum is recorded in the vortex-free state in the reference conditions and the CF peak height $A_0(\Omega_{\mathrm{ref}})$ is obtained. 2) Next a large number of vortex lines is created by irradiating with neutrons (with the rotation at Ω_{ref} or higher). 3) The sample is then decelerated to the low rotation velocity $\Omega_{\mathrm{low}} \ll \Omega_{\mathrm{ref}}$ so that part of the vortex lines are observed to annihilate. Since our long cylinder is oriented along the rotation axis only within a precision of $\sim 0.5°$, any annihilation barrier must be negligible. This means that at Ω_{low} the sample is in the equilibrium vortex state $\Omega_{\mathrm{low}} = \Omega_{\mathrm{v}}(N)$ with a known[23] number of vortex lines N. 4) Finally the rotation is increased back to the reference value Ω_{ref} and the spectrum is recorded in order to measure the CF peak height $A(\Omega_{\mathrm{ref}}, \Omega_{\mathrm{v}}(N))$. In Fig. 6 the reduction $\Delta A = A_0(\Omega_{\mathrm{ref}}) - A(\Omega_{\mathrm{ref}}, \Omega_{\mathrm{v}})$ in the CF peak height of the two spectra is plotted as a function of Ω_{v}. To reduce the dependence on drift and other irregularities we normalize the reduction ΔA to the CF peak height $A_0(\Omega_{\mathrm{ref}})$ of the vortex-free reference state. In the limit $\Omega_{\mathrm{ref}} \gg \Omega_{\mathrm{v}}$, the result is a smooth parabola. If $\Delta A / A_0$ is plotted as a function of number of vortex lines N, calculated from Ω_{v}, then the dependence is linear.

Any sample with an unknown number of vortex lines, which is less than the maximum calibrated number, can now be measured in the same reference conditions $(\Omega_{\mathrm{ref}}, T, \text{and } P)$ and compared to this plot, to determine N. In
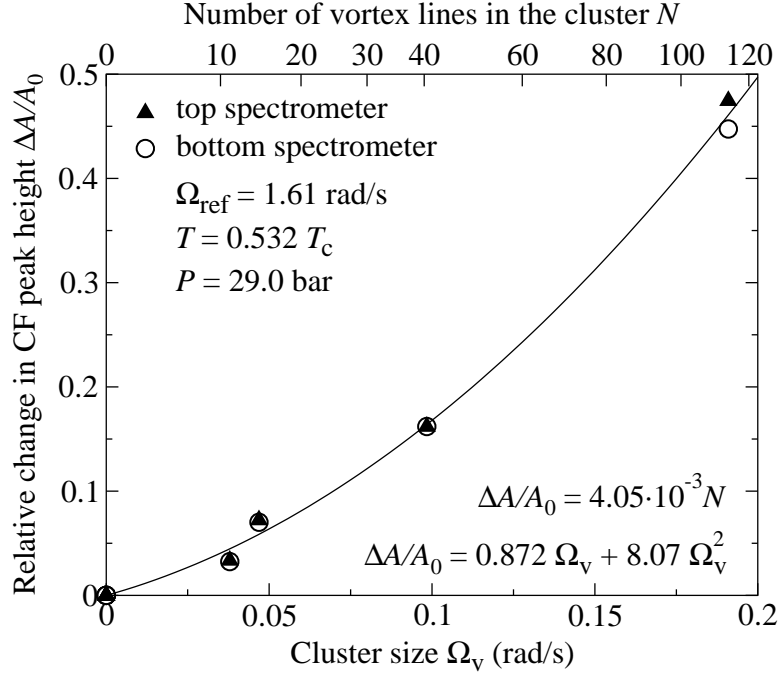
Fig. 6. Calibration of CF peak height A versus vortex line number N. The CF peak height in the vortex-free state, $A_0(\Omega_{\text{ref}})$, is compared to the peak height $A(\Omega_{\text{ref}}, \Omega_{\text{v}}(N))$, which is measured at the same rotation velocity Ω_{ref} for a small vortex cluster of size Ω_{v}, which is prepared as described in the text. The quantity plotted on the vertical scale is the relative reduction in peak heights, $\Delta A/A_0 = [A_0(\Omega_{\text{ref}}) - A(\Omega_{\text{ref}}, \Omega_{\text{v}}(N))]/A_0(\Omega_{\text{ref}})$, measured at constant conditions. The solid line is a fit, given by the expression in the figure. The conversion from Ω_{v} (bottom axis) to N (top axis) in the continuum picture is[23] $N = N_0(1 - d_{\text{eq}}/R)^2$, where $N_0 = \pi R^2(2\Omega_{\text{v}}/\kappa)$ and $d_{\text{eq}} = [(\kappa/8\pi\Omega_{\text{v}}) \ln(\kappa/2\pi\Omega_{\text{v}} r_{\text{c}}^2)]^{1/2}$. Here $r_{\text{c}} \sim \xi(T, P)$ is the radius of the vortex core. Using this conversion it is found that $\Delta A/A_0$ is a linear function of N, similar to Ref. 24.

Fig. 7 a measurement of vortex formation in neutron irradiation is shown for which the calibration plot in Fig. 6 was used. After each irradiation session at different bias flow velocity $v = \Omega R$ the rotation velocity is changed to Ω_{ref} and the NMR absorption spectrum is recorded. From this spectrum the reduction in CF peak height is determined by comparing to the spectra of the vortex-free state which are measured regularly between neutron irradiation sessions. Such a calibration is less time consuming than other methods, if the temperature is kept stable during the measurements. Its accuracy relies on (i) the stability and reproducibility of the order parameter texture, (ii)

Vortex formation in neutron irradiation

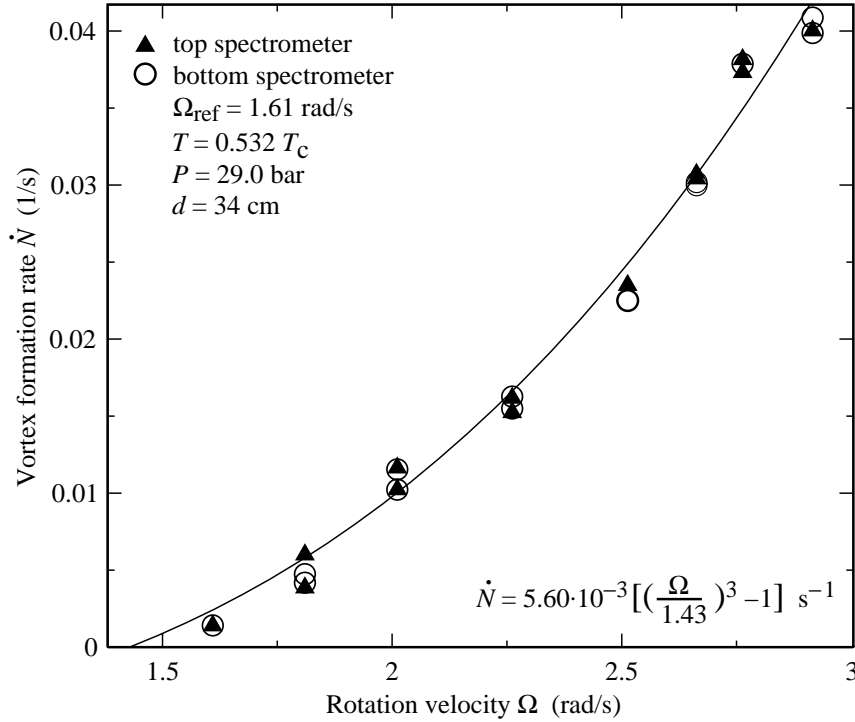$$\dot{N} = 5.60 \cdot 10^{-3}\left[\left(\tfrac{\Omega}{1.43}\right)^3 - 1\right]\ \mathrm{s}^{-1}$$

Fig. 7. Rate of vortex formation in neutron irradiation. The average number of rectilinear vortex lines created per unit time during the irradiation period is shown as a function of the rotation velocity Ω. The data are fitted with the expression $\dot{N} = 0.336\left[(\Omega/1.43)^3 - 1\right]\,\mathrm{min}^{-1}$ (with Ω in rad/s). Depending on the rate $\dot{N}$, the irradiation time varies here from $30\,\mathrm{min}$ to $4.5\,\mathrm{h}$, so that the number of accumulated vortices remains within the range of the calibration in Fig. 6. This calibration is used to determine the number of vortices from the relative reduction in the CF peak height, $\Delta A/A_0$. The distance[10] of the neutron source from the sample was $d = 34\,\mathrm{cm}$. The range of the bias flow is limited in these measurements between the critical velocity $\Omega_{\mathrm{cn}} = 1.43\,\mathrm{rad/s}$ and the upper limit $\Omega = 3.0\,\mathrm{rad/s}$, where the turbulent events start to occur.

the precision with which the definition of the cluster size is achieved (ie. the stability of rotation at Ω_{v}), and (iii) the validity of the continuum model and absence of annihilation barrier at small vortex numbers ($N \sim 10 - 100$).

3.2. Measurement of vortex formation rate

In Fig. 7 the rate of vortex formation $\dot{N}$ in neutron irradiation is measured at $0.53\,T_{\mathrm{c}}$ as a function of the bias velocity $v = \Omega R$. The result

supports the cubic rate equation (22) at a lower temperature than has been reported previously. The critical velocity $v_{cn} = \Omega_{cn}R = 4.3\,\text{mm/s}$ is consistent with the values measured previously at pressures up to $21.5\,\text{bar}$ and temperatures above $0.80\,T_c$. This is plausible if the critical velocity is determined only by the size of the neutron bubble which does not change appreciably with decreasing temperature, Eq. (8). However, the rate factor γ is 36 times smaller than in earlier measurements above $0.8\,T_c$ and at lower pressures. It is at present not known how γ and v_{cn} vary at high pressures when a wide range of stable A phase exists between T_c and the ambient B-phase bath temperature T_0. One might expect that the much enhanced probability of A phase nucleation in different parts of the neutron bubble reduces the volume occupied by the B phase.[19] In this situation the B-phase vortex network would be limited to a smaller volume and perhaps fewer vortex loops would be extracted into the bias flow. In such a case one might expect v_{cn} to increase and γ to be reduced.

A second similar measurement at $P = 10.2\,\text{bar}$ and $T = 0.57\,T_c$ gives a critical velocity $v_{cn} = 3.6\,\text{mm/s}$ and a rate constant γ which is 3 times larger than the measurement in Fig. 7. At $10\,\text{bar}$ pressure A phase is not stable. Since turbulent events at higher bias velocities interfere with these measurements, the available range of bias velocities (approximately $v_{cn} < v \lesssim 2\,v_{cn}$) is smaller than in the measurements at higher temperatures, see Fig. 2. Nevertheless, both of these low temperature measurements support the cubic form of the rate equation. In the absence of more extensive work as a function of pressure and temperature, the reasons for the reduced rate factor γ remain so far unexplained.

3.3. Superfluid turbulence in neutron irradiation

At high rotation and temperatures below $0.60\,T_c$ neutron irradiation events may become turbulent,[25] similar to vortex formation from other sources. This means that vortex loops, which have been extracted from the neutron bubble and are injected into the bias flow, may start to interact, to produce a vortex network of large scale. This tangle then blows up and fills the rotating sample with the equilibrium number of vortex lines. Some NMR characteristics of such a neutron capture event are illustrated in Fig. 8. However, the fundamental feature is that the sample is suddenly filled with the equilibrium number of rectilinear vortex lines, apparently as a result of one neutron capture event: The NMR absorption spectrum jumps (via a brief transitory period) from a line shape with a large CF peak to that of the rotating equilibrium state of totally different form (Fig. 5).

Vortex formation in neutron irradiation

Turbulent events are observed in neutron irradiation only if (i) the rotation velocity exceeds Ω_{cn} and (ii) the temperature is sufficiently low so that vortex motion is not heavily damped by mutual friction. Even then these processes are stochastic such that the vortex loops extracted from the neutron bubble only rarely achieve the proper initial conditions in which turbulent loop expansion starts to evolve. With decreasing temperature and increasing rotation the probability of turbulent events increases. This may be understood since: (i) With decreasing temperature mutual friction damping is reduced, Kelvin wave excitations grow in amplitude, more new loops are formed on the existing lines, and via reconnection processes the intersecting loops multiply to a turbulent cascade. (ii) With increasing bias velocity the number of vortex loops, which are injected into the bias flow, rapidly increases (Fig. 2, bottom) and the probability of their intersections increases.

Fig. 8 illustrates how the height of the CF peak suddenly drops to zero in the NMR spectrum when a turbulent event starts to evolve. In this schematic example the turbulent tangle first appears inside the bottom coil. The collapse of the CF peak height is the first feature in the NMR absorption spectrum which signals the turbulence: Its rapid decay shows that the turbulent state becomes polarized, to mimic on an average solid-body rotation. Simultaneously the NMR absorption intensity from the CF peak is transferred close to the Larmor edge of the spectrum where a new sharp peak rapidly grows in intensity. This peak then slowly decays to the line shape of the equilibrium state, see Fig. 5. The intensity in the Larmor region reflects how the vortex density evolves within the coil:[25] It first rapidly overshoots to a value which is about twice that in equilibrium and then slowly rarefies to the equilibrium value.

The decaying CF signals from the two coils do not overlap in Fig. 8. Even the more slowly relaxing overshoots in the Larmor region do not overlap in time when $T < 0.5T_{\mathrm{c}}$ and turbulence is initiated at one end of the sample tube. This means that the turbulence propagates along the liquid column as a stratified layer: By the time the NMR absorption in the top coil gives the first indication of the approaching turbulent front, the bottom coil has already settled into its stable equilibrium line shape. Thus the turbulent front is formed by a relatively thin layer of disordered tangle, in which the polarization of the circulation reaches its final equilibrium value, before the vortex density and the configuration of the vortices has stabilized. The front moves along the column with a fixed velocity which was measured in Ref. 26. This velocity has the same value as that of a single short section of vortex filament moving along the cylinder wall in the initial vortex-free bias flow: $v_{\mathrm{z}} = \alpha \Omega R$. Here α is the dissipative mutual friction coefficient which was
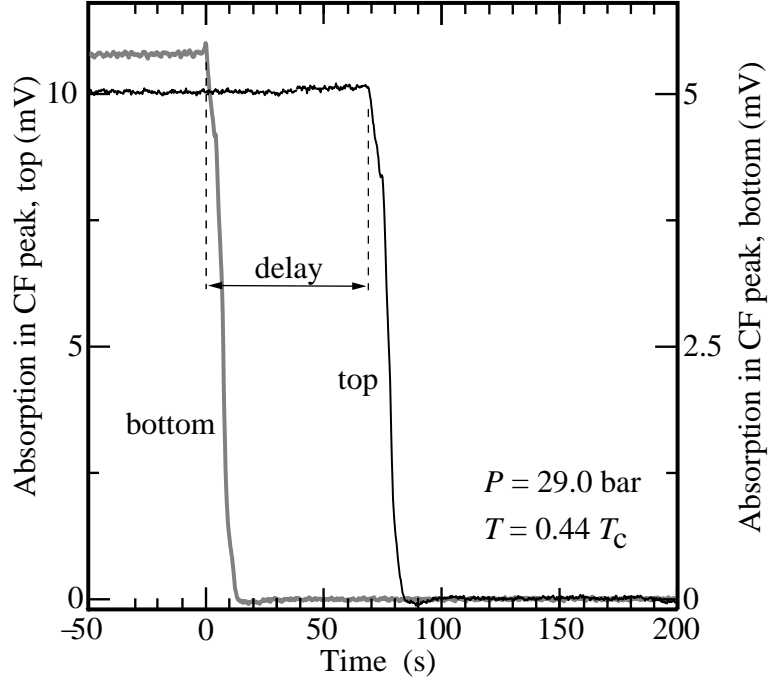
Fig. 8. NMR signatures of a vortex formation event which evolves into superfluid turbulence. When a vortex tangle expands into one of the NMR detection coils, the height of the CF peak (Fig. 5), which is monitored in this plot, rapidly drops to zero. The sequence of events is schematically displayed here at $\Omega = 1.61\,\mathrm{rad/s}$ when a sudden collapse of the CF peak is first observed in the bottom spectrometer (at $t = 0$). After a delay of 70 s, which the turbulent front needs to travel to the lower edge of the top coil 90 mm higher along the liquid column, a similar collapse is recorded by the top spetrometer. This value of delay corresponds to the situation when the turbulence is first formed in the middle of the bottom coil. The sudden collapse of the CF peak means that the turbulent vortex tangle is rapidly polarized in rotation and that the global counterflow between the normal and superfluid components is thereby removed. Measurements of this type show that from the initial injection site, where the injected vortex loops first start to intersect in the bias flow, the turbulence expands in the rotating column by forming two turbulent fronts which move at constant velocity towards the top and bottom ends of the sample.

measured in Refs. 26–27. This means that from the delay between the signals of the two detector coils (as marked in Fig. 8), we may calculate the axial location z where the turbulent event started. This location has been plotted

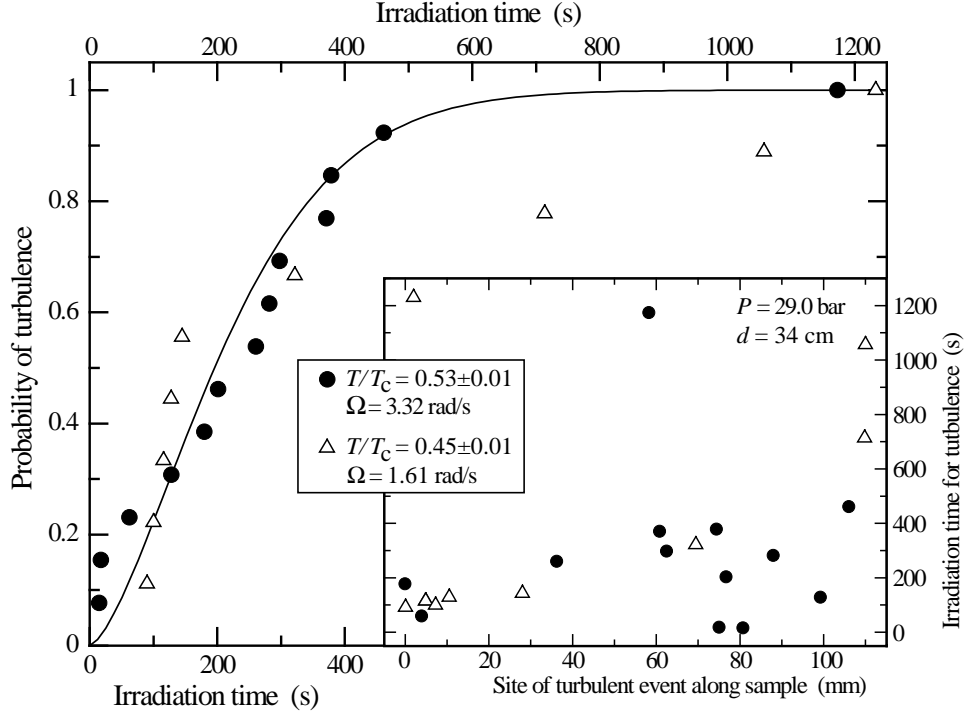**Vortex formation in neutron irradiation**

Fig. 9. Turbulent vortex formation in neutron irradiation at 29.0 bar pressure. The sample is irradiated in constant conditions until a turbulent vortex expansion event takes place. The irradiation time required to achieve the turbulent event is measured. Results from measurements at two different constant conditions are shown in this plot in the form of cumulative probability distributions. For comparison, the continuous curve represents a distribution function of the Weibull extreme-value form:[1] $P(t) = 1 - \exp[(-t/250\,\mathrm{s})^{1.5}]$. There were no cases among the two sets of measurements where a turbulent event would not have been observed after an irradiation period of 20 min. The *inset* shows the axial location of the initial turbulent seed, the site of the neutron capture, measured from the orifice upward with a technique explained in Fig. 8. The corresponding irradiation time needed to achieve the event is shown on the vertical axis. As expected, the sites are randomly distributed along the sample.

for the data in Fig. 9 in the inset of this figure.

The probability of a neutron capture to trigger a turbulent process is studied in Fig. 9. Two measurements are shown of the cumulative probability distribution of the irradiation time needed to achieve a turbulent event. In these two examples at different temperatures and rotation velocities the

sample is irradiated at constant conditions until the CF peak is observed to collapse suddenly. The irradiation time is plotted on the horizontal axis. On the vertical axis the number of turbulent events observed within this time is shown, normalized to the total number of events: 13 events in one case (at $0.53\,T_c$) and 9 in the second (at $0.45\,T_c$). As seen from the plot, the number of events is insufficient to produce smooth probability distributions, but the irradiation times are observed to be distributed over the same range in the two cases, *ie.* their distributions have similar average values and widths. This in spite of the fact that the measurements at $0.45\,T_c$ were performed at half the rotation of those at $0.53\,T_c$. At high temperatures a reduction by two in velocity results in a significant decrease in the yield of vortex lines from one neutron absorption event, Fig. 2. The fact that the two distributions in Fig. 9 do not differ significantly indicates that with decreasing temperature the transition to turbulence becomes more probable and less sensitive to the initial configuration of the injected loops.

Let us consider the measurement at $0.53\,T_c$ in more detail. The state of the sample changes during the irradiation at constant Ω: (i) the initial state is vortex-free, (ii) during the irradiation rectilinear vortex lines are formed at a rate which can be extrapolated from Fig. 7, (iii) until finally all vortex-free CF is completely terminated in a turbulent event. In the final step the state of the sample changes from one with only a small central vortex cluster to one with the equilibrium number of vortex lines ($N_{eq} \sim 2600$). Note that to observe a new turbulent event the existing vortices have to be annihilated, by stopping rotation. Then the vortex-free state can be prepared again and a new irradiation session can be started. The longest irradiation time is here $\sim 20\,\text{min}$. During this period the cluster grows at the rate $\dot{N} = 3.9\,\text{vortices/min}$, so that it contains about 80 vortices when the turbulent event finally starts. At this point the CF velocity at the sample boundary $v = v_n - v_s = \Omega R - \kappa N/(2\pi R)$ has been reduced by $2.7\,\%$ from the initial state. Since the mean irradiation time in the measured distribution is only $\sim 250\,\text{s}$, the reduction in CF velocity by vortices formed before a turbulent event is minor. We may thus view the result in Fig. 9 as representative of these particular values of rotation and temperature.

One may wonder whether a turbulent process results from a single neutron capture event or from the coincidence of two or more events. In the latter case the simultaneous events need to be sufficiently close not only in time, but also in space, so that the expanding loops, which are already extracted from the two neutron bubbles, have a possibility to intersect. (The probability of the bubbles themselves to intersect is very small.) The intersection of the loops expanding from the two random positions along the height of the cylindrical sample is more likely to occur closer to the mid-

dle than at the top or bottom end. However, the events listed in the inset of Fig. 9 occur randomly along the sample. In all cases the NMR signatures from the turbulent events are similar, there is no prominent variation in their appearance depending on where the event starts. Additionally, at lower temperatures, the turbulent events occur close above Ω_{cn}. Here successful neutron absorption events, which lead to the extraction of loops to the bulk, are rare but, nevertheless, turbulent events become more probable. From this we presume that a single neutron capture event in suitable conditions must be able to start a turbulent expansion event. For a more careful proof of this point the measurements should be repeated as a function of the neutron flux.

4.   SUMMARY

Neutron irradiation of vortex-free superflow has become a practical means of creating quantized vortices in ^{3}He-B. Detailed knowledge exists on many of the experimental features, although more measurements are needed at intermediate temperatures and pressures, to explain the vortex formation rate as a function of the bias flow velocity in all situations. At low temperatures neutron irradiation is a useful method for the localized injection of vortex loops into vortex-free superflow, to study superfluid turbulence.

As to the explanation for the neutron-induced vortex formation, the measurements undoubtedly support a volume effect: The vortex loops escaping into the bulk superflow originate from a random vortex network which forms in the interior of the neutron bubble when it rapidly cools through the superfluid transition. The validity of this Kibble-Zurek mechanism of vortex formation is also confirmed by current numerical simulations of the time-dependent Ginzburg-Landau type. However, these calculations identify the superflow instability at the surface of the warm neutron bubble as the source for those vortex loops which manage to escape into the bulk superflow. To examine the interplay of these two mechanisms, it would now be instructive to perform quench-cooling experiments as a function of the cooling rate. Rapid localized overheating can be achieved with laser pulsing, as has been demonstrated by H. Alles et al.[28] Such measurements would probe cooling rates which are slower than after a neutron absorption event, but might reveal, for instance, a change over from the volume to the surface mechanism with decreasing cooling rate.

5. POSTSCRIPT

While we were running our experiments with the rotating refrigerator, the retired director of our laboratory, Olli Lounasmaa, used to stroll late in the evenings to the control table of our rotating cryostat and test his ideas on us: "The two most outstanding challenges to research are the Universe and the Human Brain," he said. "In two hundred years from now our successors will not be interested in studying superfluid helium - all that you need to know about it has already become common knowledge. But they will still try to understand the secrets of the Universe and they will still continue wondering whether their Brain will suffice to grasp all the essence of the Cosmos."

Nevertheless, Olli was impressed by the bridge which was created by superfluid helium measurements and their interpretation to current ideas borrowed from cosmology - he supported such physical generalization wholeheartedly. After all, it was him who originally had the courage in 1976 to apply for funding to construct a rotating cryostat for the sub-mK temperature range. His legacy to us was to set an example of interminable energy to tackle new research challenges. Right now this is needed while one wonders whether superfluid turbulence in ^{3}He-B can be explained based on the existing knowledge and expertise. This is just one of the many important problems to be solved before helium superfluids can be declared to be understood.

REFERENCES

1. M. Niemetz, W. Schoepe, *J. Low Temp. Phys.*, this issue.
2. V.M.H. Ruutu *et al.*, *Nature* **382**, 334 (1996).
3. T.W.B. Kibble, *J. Phys. A* **9**, 1387 (1976).
4. W. Zurek, *Phys. Rep.* **276**, 177 (1996).
5. C. Bäuerle *et al.*, *Nature* **382**, 332 (1996).
6. V.M.H. Ruutu *et al.*, *Phys. Rev. Lett.* **80**, 1465 (1998).
7. V.B. Eltsov *et al.*, *Phys. Rev. Lett.* **85**, 4739 (2000).
8. G.W. Rayfield, F. Reif, *Phys. Rev.* **136**, A1194 (1964).
9. M.E. Dodd *et al.*, *Phys. Rev. Lett.* **81**, 3703 (1998).
10. V.B. Eltsov *et al.*, cond-mat/9809125.

Vortex formation in neutron irradiation

11. Ü. Parts *et al.*, *Europhys. Lett.* **31**, 449 (1995); V.M.H. Ruutu *et al.*, *J. Low Temp. Phys.* **1**07, 93 (1997).
12. R.J. Donnelly, *Quantized Vortices in Helium II* (Cambridge University Press, Cambridge, UK, 1991).
13. T. Vachaspati, A. Vilenkin, *Phys. Rev.* D**30**, 2036 (1984).
14. T.W.B. Kibble, G.E. Volovik, *JETP Lett.* **65**, 102 (1997).
15. I.S. Aranson, N.B. Kopnin, V.M. Vinokur, *Phys. Rev. Lett.* **83**, 2600 (1999); *Phys. Rev.* B**63**, 184501 (2001).
16. A.J. Leggett, *J. Low Temp. Phys.* **126**, 775 (2002).
17. V.M. Ruutu *et al.*, *Czechoslovak J. Phys.* **46**-Suppl., Pt. S1, 15 (1996).
18. R. Blaauwgeers *et al.*, *Phys. Rev. Lett.* **89**, 4739 (2000).
19. Yu.M. Bunkov *et al.*, *Phys. Rev. Lett.* **80**, 4927 (1998); *J. Low Temp. Phys.* **110**, 45 (1998).
20. P.E. Schiffer *et al.*, *Rev. Mod. Phys.* **67**, 491 (1995); in *Prog. Low Temp. Phys.*, Vol. XIV, p. 159, ed. W.P. Halperin (Elsevier Science Publ., Amsterdam, 1995).
21. R. Blaauwgeers *et al.*, *Physica* B**329-333**, 93 (2003).
22. A.P. Finne *et al.*, to be published.
23. V.M. Ruutu *et al.*, *Physica* B**255**, 27 (1998).
24. Wen Xu *et al.*, *Czechoslovak J. Phys.* **46**-Suppl., Pt. S1, 11 (1996).
25. A.P. Finne *et al.*, *Nature* **424**, 1022 (2003).
26. A.P. Finne *et a.*, *J. Low Temp. Phys.* **134**, 375 (2004).
27. T.D.C. Bevan, *J. Low Temp. Phys.*, **109**, 423 (1997).
28. H. Alles *et al.*, *Phys. Rev. Lett.* **74**, 2744 (1995).